IEEE Access
Multidisciplinary | Rapid Review | Open Access Journal

Date of publication xxxx 00, 0000, date of current version xxxx 00, 0000.

Digital Object Identifier 10.1109/ACCESS.2017.Doi Number

A Wide-angle, Enhanced Oblique Incidence, Bend-able Metamaterial Absorber Employed in Visible Region with a Sun Shape Resonator

MD MIZAN KABIR SHUVO[1], MD IMRAN HOSSAIN[1], SYDUR RAHMAN[2], SULTAN MAHMUD[3,4], SIKDER SUNBEAM ISLAM[3], (Member, IEEE), AND MOHAMMAD TARIQUL ISLAM[4], (Senior Member, IEEE)

[1] Department of Electrical and Electronic Engineering, Mymensingh Engineering College, University of Dhaka, Bangladesh
[2] Department of Electrical and Electronic Engineering, Bangladesh University of Engineering and Technology, Bangladesh
[3] Department of Electrical and Electronic Engineering, International Islamic University Chittagong, Bangladesh
[4] Department of Electrical, Electronic & Systems Engineering, Faculty of Engineering & Built Environment, Universiti Kebangsaan Malaysia, 43600 Bangi, Selangor, Malaysia

Corresponding author: Sultan Mahmud (e-mail: sultaniiuc3ni@gmail.com), and Mohammad Tariqul Islam (tariqul@ukm.edu.my)

This work was supported by the Universiti Kebangsaan Malaysia research grant DIP-2021-012.

ABSTRACT Solar spectrum is supposed to be a key source of renewable energy in the form of electromagnetic (EM) radiation. For efficiently harnessing this abundant energy, Metamaterial Absorber (MMA) emerges as a game-changing tool. Along with solar energy harvesting, MMA can be used in biochemical sensors, optical modulators, magnetic resonance imaging, photoelectric detectors, plasmonic sensors, etc. In this paper, a sun shape resonator-based MMA is designed with three layers of materials (W-SiO_2-W) and analysed for broadband absorption encompassing the entire visible region (390-760nm). The unit cell that is presented in this study is polarization-insensitive and ultrathin with an average absorption of 96.43% with an optimum peak of 99.99% at 523.22nm. The proposed MMA exhibits satisfactory absorption under various oblique angles. The effect of mechanical loading is also investigated and the MMA is found to hold good broadband absorbance for some extents of mechanical bending. Finite Integration Technique (FIT) is used to numerically simulate the proposed MMA unit cell structure and validated with the Finite Element Method (FEM). The suggested MMA in this paper can be used in many optical applications like efficient nano solar cells, imaging applications, sensors, light detectors, biochemical applications, etc.

INDEX TERMS Solar spectrum, Energy harvesting, Metamaterial absorber, Impedance match, Optical Applications

I. INTRODUCTION

Metamaterials are short of engineered blended structure or synthetic substance that has remarkable electromagnetic effects that common elements lack, and experimentation on such materials has received considerable interest and advancement in the past few years [1], [2]. Since V.G. Veselago first proposed the concept of vision about metamaterial in 1968 [3]. Numerous engineering applications make use of metamaterials, including perfect lens [4], [5], optical cloaking [6], thermal imaging [7], [8], electromagnetic shielding [9], antennas [10], [11], filters [12], holograms [13][14], absorber [15], [16], sensors [17]–[19], modern communication system [20], [21]. The "perfect absorber" of electromagnetic waves is an appealing application area for metamaterials [22], [23]. For microwave, THz, and also optical applications, different types of MMA have been enrolled in numerous electromagnetic wave mediums, such as single-band [24], multi-band [25], [26][27], narrow-band [28], broadband [29], [30], polarization-sensitive [31], polarization-insensitive [32], [33]. In the bandwidth of solar radiation, a wideband comprehensive MMA comes belonging a three-layer structure called a unit cell, which consists of metal-dielectric-metal layers and the topmost layer that holds a

This article has been accepted for publication in a future issue of this journal, but has not been fully edited. Content may change prior to final publication. Citation information: DOI 10.1109/ACCESS.2021.3111813, IEEE Access

geometric pattern called a resonator. The transmitting of electromagnetic (EM) waves is terminated by the bottom metal film of the structure. In the center of the metal and the resonator plate, the dielectric layer aids the model in producing a capacitance that helps in coupling [34]–[36]. If the free space impedance is equal to the meta-surface impedance, the incident wave will be reflected as little as possible [37] and the desired absorption is achieved.

A broadband three-layer MMA made with Tungsten and Nickel had been studied in this article [38] that has an average absorption above 80% from 478nm to 697nm with incident angle stability up to 45 degrees. A wideband three-layer perfect MMA based on Nickel and Silicon dioxide has an absorption level of more than 90% with incident angle stability of 60 degrees from 390nm to 697nm regions[39]. A hybrid resonator-based three-layer MMA in the visible region made with Aluminium and Silicon dioxide has average absorption of 95% from 450nm to 600nm [40]. Article [41] dealt with an MMA operating in the visible light region that covers 490nm to 825nm with absorption above 90% made with Silver and Aluminium dioxide. An ultra-thin multi-band MMA with a wide-incident angle up to 45 degrees consists of Tungsten and Quartz, having an absorption level above 66.66% from 374nm to 750nm [42]. In article [43] a tri-layer perfect MMA made with Au and SiO_2 with an absorption level of more than 90% from 506nm to 573nm. A Gold resonator-based dual-band visible light absorber [44] that has an absorption level above 40% in the bandwidth of 210nm. Article [45] claims an investigation on the broadband metamaterial absorber which is studied numerically based on Tungsten and silicon dioxide, in the optical light regime that has average absorption above 90% from 404nm to 631nm with incident angle stability up to 30 degrees.

Based on the ideas presented above, a metamaterial-based perfect absorber for the entire visible regime has been suggested, with different implementations in the associated field. According to the literature we reviewed, MMA having an absorption of up to 95% on average in TE and TM mode with a precise incident angle of more than 50° is difficult to attain. In this article, we proposed a unique symmetrical balanced MMA structure made of such materials that have a high degree of temperature independence like W and SiO_2 which has shown an average absorption of 96.43% from 390 nm to 760 nm. The effects of mechanical stress on the proposed structure are investigated in this article. The electric and magnetic fields of the unit cell for both resonance and non-resonance modes are analysed with proper explanation. The proposed model has an absorption level of 90.20% all the times. This MMA shows almost perfect absorption of 99.99% at 523.22 nm and over 99% absorption from 479 to 575 nm. In TEM mode, all of the desired effects are taken into account. The results of the simulation for the whole area were checked using the Finite Element Method (FEM).

II. MATERIALS SELECTION DESIGN AND SIMULATION

The proposed structure is made of three different layers of films. The resonator layer, as well as the ground slab, are placed at the two opposite faces with a dielectric spacer sandwiched between them. Tungsten (W) is used as the resonator layer and ground slab for the suggested unit cell. The dielectric layer consists of Silicon dioxide (SiO_2) which is the middle layer. Both the materials are selected from the CST material database in which the wavelength-dependent refractive indices for Tungsten and SiO_2 are 1.7073 and 1.4611, respectively. High loss metallic material and small bandgap dielectric material are appealing options for designing absorbers in recent days [46]. Tungsten possesses high intrinsic loss which causes the transmission through the ground slab almost null and reduces the reflection throughout the entire unit cell [47]. Thus intrinsic loss aids in broadband absorption for tungsten naturally in the visible region by a very good impedance matching with the free space by the suggested structure [48]. Now, the dielectric film is selected to be SiO_2 because of its lossless feature. At the visible spectrum, SiO_2 also has a relatively negative real component of permittivity instead of a large imaginary portion of the dielectric constant [49]. As a consequence, the real part of permittivity gets null in the breakdown stage, allowing the propagating wave for an evanescent wave characteristic to become more closed. As the birefringence nature of dispersion relation with the refractive index for SiO_2, this anisotropic nature likewise helps to polarization as well as propagation control through the substrate. The chosen material satisfies the prerequisites as a dielectric. SiO_2 aids the absorption property by affecting the coupling capacitance as well as inductance associated with the resonator and ground plate in a beneficial aspect. In addition, the thermal stability of the unit cell becomes excellent because of the chosen material as the melting point of SiO_2 and W is very high with a value of 1600°C and 3410°C, respectively.

Fig. 1, shows the step-by-step design approach of the suggested absorber. The design is three-layer sun-shaped that consists of two types of material (W-SiO_2-W), which might make it easier in the fabrication stage. The W is indicated with red color and the light pastel purple color indicates the SiO_2. In order to achieve near-unity absorption, the resonator and the dimensions play a crucial role [28]. The polarization insensitivity and close to zero polarization conversion ratio of an absorber mainly depends on the design symmetry. So, the design approach for this cell was to make it symmetric. The total dimension of the structure is (450*450*220) nm^3. The design procedures are shown in Fig. 1(a)-(d), and the dimension measurements of the front and side view are shown in Fig. 1(e) and (f), respectively. Firstly, the dielectric spacer and base metal layer were applied in the design with an area of (380*380) nm^2, where the corresponding depth of the dielectric spacer and base metal are “tr = 55nm” and “tg = 150nm”. The base metal -

This article has been accepted for publication in a future issue of this journal, but has not been fully edited. Content may change prior to final publication. Citation information: DOI 10.1109/ACCESS.2021.3111813, IEEE Access

TABLE 1. Parameter list of the proposed unit cell.

Parameters	L	L1	L2	R1	R2	R3	R4	t1	t2	g1	g2	g3	tr	tg	ts
Value (nm)	450	420	360	30	80	100	150	50	53.18	27.9	67	20	15	150	55

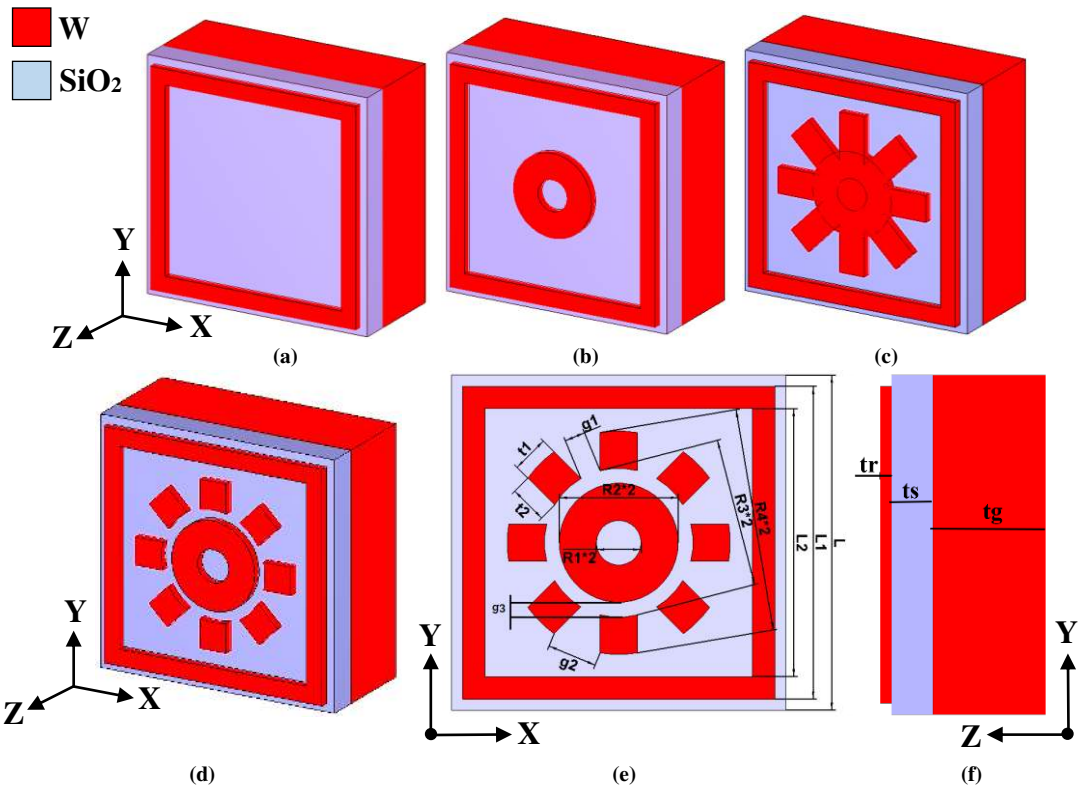

FIGURE 1. Design composition and parameter of the proposed model in (a) step -1 with a square shape, (b) step -2 with a square shape and cylindrical shape, (c) step – 3 with star shape, (d) final model with a sun shape resonator, (e) front view with parameter, and (f) side view with thickness.

depth is higher than the skin depth to block S_{21} from the scattering parameter, where S_{21} is the transmission coefficient [50]. And then at step 1, a square box resonator of inner and outer arm length of "L2 = 360" and "L2 = 420" was placed. At step 2, a cylindrical shape was inserted into the system with an inner and outer radius of "R2= 30nm" and "R1= 80nm". After that at step-3, eight rectangles are inserted into the system with an angular shift of 45° of each other. The base rectangle must have to be set parallel to x or y-axes. The length and width of each rectangle are "2*R4= 300nm" and "t1= 50nm", respectively. At last, at step-4, a cylindrical shape of an outer and inner radius of "R3= 100nm" and "0nm" is trimmed out from those eight rectangles. For all the four steps to designing the resonator, the depth is chosen as "tr= 15nm".

Here, under electromagnetic Finite-Difference-Frequency-Domain (FDFD) solver Finite Integration Technique (FIT) is applied to the proposed unit cell for extracting desired S parameters and associated data depends on it. The unit cell is observed under three analyzing techniques called Transverse Electromagnetic (TEM), Transverse Electric (TE), and Transverse Magnetic (TM) along with desired boundary conditions. In TEM mode the y-z plane, x-z plane, and x-y plane are kept as perfect electric, perfect magnetic, and open add space chronologically where all three planes are perpendicular to each other. The other two analyzing techniques (TE, TM) are also applied with valid boundary conditions such as the floquet port in the z-direction and master and slave working on the other two directions (X, Y) respectively.

III. RESULTS ANALYSIS AND DISCUSSION

A. METHODOLOGY

A broadband metamaterial absorber performance depends on the overall absorption in the desire frequency band. Here, the Finite Integration Technique (FIT) by Computer Simulation Technology (CST) is used to extract the possible outcome from the proposed metamaterial broadband absorber. To extract S parameters from the proposed absorber, the boundary condition is applied to the unit cell in the x as well as y-direction and z-direction being kept as open add-space. By analyzing the magnitude of the S parameters as reflection

This article has been accepted for publication in a future issue of this journal, but has not been fully edited. Content may change prior to final publication. Citation information: DOI 10.1109/ACCESS.2021.3111813, IEEE Access

coefficient $S_{11}(\omega)$ and transmission coefficient $S_{21}(\omega)$. Absorption A (ω) can be found through a mathematical relation (1) with S_{11} and S_{21}.

$$A(\omega) = 1 - |S_{11}(\omega)|^2 - |S_{21}(\omega)|^2 \quad (1)$$

To obtain maximum absorption, reflection coefficient $S_{11}(\omega)$ and transmission coefficient $S_{21}(\omega)$should be kept as low as possible. Zero transmission can be achieved by using a metal plate that has a skin depth enough to block the penetration of light waves. In the proposed model, Tungsten(W) is used as a ground to prevent light penetration i.e., $S_{21} = 0$, (1) can be rewritten as (2)

$$A(\omega) = 1 - |S_{11}(\omega)|^2 \quad (2)$$

as A (ω) is improved by (2) for more desire absorption, reflection coefficient $S_{11}(\omega)$ need to be kept low as much as possible. S_{11} will be minimum if the free space impedance matches with the resonator layer impedance of the absorber top surface. It is known that free space impedance $Z_o = 377\Omega$ or 120π so input impedance $Z(\omega)$ of proposed absorber need to be equal or nearly equal to Z_o. Input impedance $Z(\omega)$ depends on the effective permittivity and permeability of the metamaterial structure that can be analyzed by applying the Nicolson-Ross-Weir (NRW) equation [51]. The bottom layer as well as the tungsten-based resonator array can have a high near-field coupling. When this coupling is taken into account, the theoretical findings generated using the interference model correspond quite well with numerical simulations. It works based on impedance matching to free space due to destructive reflection interference, in addition to the ground plane's zero transmission, The structure of our proposed metamaterial absorbers is comparable to that of a lossy high impedance surface that is capable of high absorption. Another fact for flawless absorption is the geometry-based surface, which is perfectly distributed with electric-field and magnetic-field charges.

B. CHARACTERISTICS OF ABSORPTION

The absorption characteristics of the suggested structure are illustrated in Fig. 2(a) ranging from ultraviolet to near-infrared spectrum encompassing the entire visible region for a wavelength span of 300nm to 1000nm. Three modes are used to describe the characteristics named, TE mode, TM mode, and TEM mode. The absorption characteristics for these modes are quantified by (1), from the s-parameter which was obtained during the simulation of the proposed structure. The maximum absorption occurs at 523.22nm with absorption of 99.99% for TEM mode. For TE and TM mode, the peak absorption occurs at 523.56nm with 99.99% absorption, and 523.91nm with 99.99% absorption, respectively. The absorption characteristics are almost similar for the three modes because of the ultra-symmetrical design throughout the entire structure. In this study, the main focus will be on the absorbance characteristic only in the visible region with a wavelength span of 390nm to 760nm. This wavelength span covers almost the entire visible spectrum radiated by the sun. The average absorption for this domain is found to be very excellent with a value of 96.43% for TEM mode. The average absorptions for TE and TM mode are almost the same value that for TEM mode, with a value of 96.4%, and 96.48%, respectively, for the symmetric structural design. The absorption levels for the edge wavelengths (390nm, and 760nm) for TEM mode are 90.84%, and 90.21%, respectively. In addition, the suggested structure exhibits an average absorbance above 99% from 479.1nm to 575.05nm. Thus, the near-unity absorption band becomes 95.96nm. These features indicate that the structure proposed in this paper can be used as a perfect solar energy harvester in the visible range of the solar spectrum, sensors, stealth technology, and micro-imaging technology [52].

The reason for achieving perfect absorption characteristics for the proposed structure lies behind the values of the real component as well as the imaginary component which is associated with the normalized impedance. Fig. 2(b) illustrates the normalized impedance for the proposed structure which is the ratio of the total effective impedance of the suggested architecture to the impedance of the free space. It is a general concept that the absorption will be high if the normalized impedance real component reaches near unity, and the imaginary component becomes null as the effective impedance of the structure matches with the free space impedance [53]. This phenomenon is seen at the resonance wavelength of 523.22nm in which the real component of the normalized impedance takes the value of one and the imaginary component becomes null. This perfect absorption in this band occurs due to the perfect impedance matching between this region which is evident from Fig. 2(b).

The entire unit cell structure can be divided into two layers named, front-layer and ground slab or the back-layer. The tungsten-made resonator and SiO_2-made dielectric spacer consist front layer of the structure. The ground slab consists of tungsten also. The absorbance associated with the front and ground slab is depicted in Fig. 2(c). The ground slab blocks the incident radiation so that the radiation in the form of electromagnetic waves becomes unable to pass through the ground layer. The absorption due to the ground slab lies around 50% with an average absorption of 51.2%. This is because surface plasmons do not function in the tungsten-made ground slab. The front layer has an absorption that lies around 46% approximately. The reason for this is that the tungsten-made resonator has high intrinsic loss which aids in high impedance matching for the proposed structure. The SiO_2 dielectric film has a very small gap that affects the resonance characteristics which results in aiding the absorption. The combined absorption of the front layer and ground slab gives the total average absorption of 96.43% for the selected visible domain. However, this good average absorption is due to the excellent symmetry of the proposed-

This article has been accepted for publication in a future issue of this journal, but has not been fully edited. Content may change prior to final publication. Citation information: DOI 10.1109/ACCESS.2021.3111813, IEEE Access

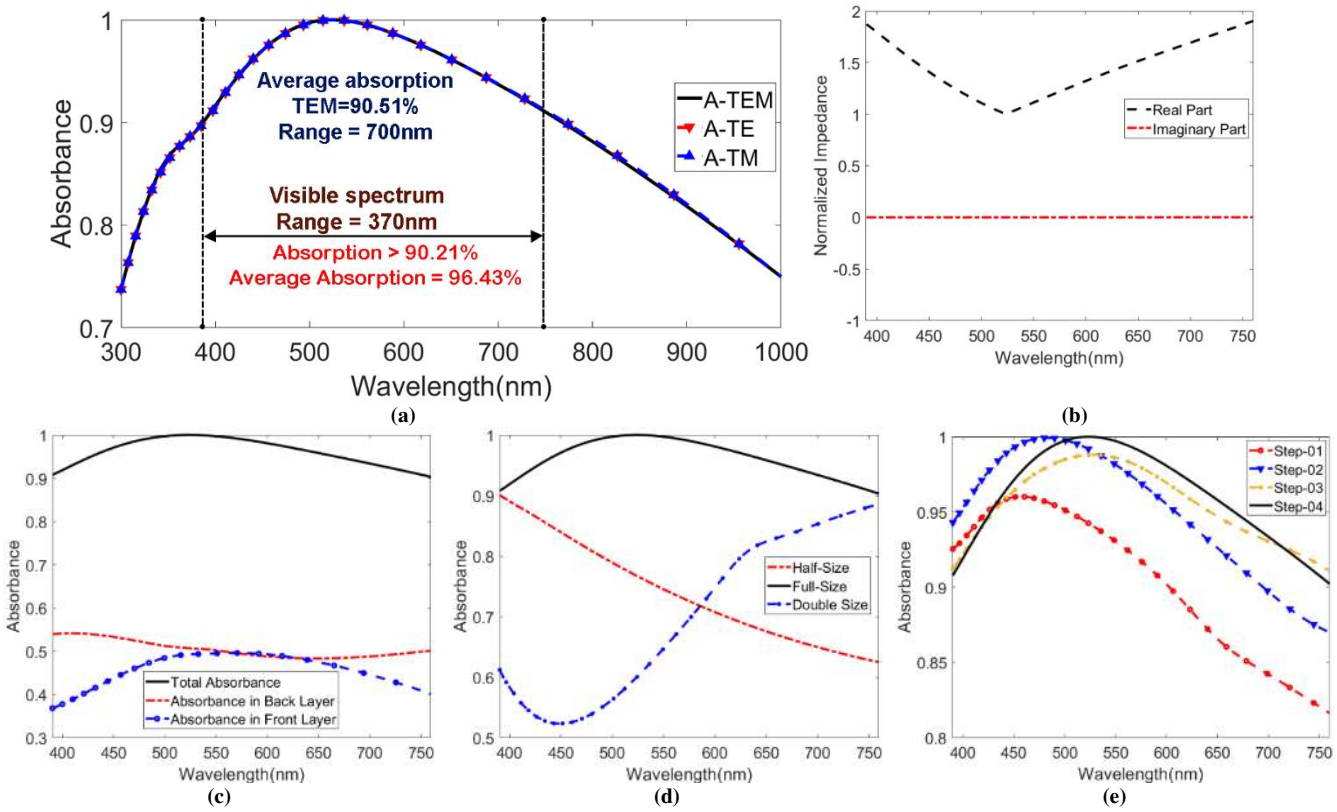

FIGURE 2. Demonstration of (a) absorbance in TEM, TE, and TM mode, from 300 to 1000nm, (b) normalized impedance with real and imaginary parts, (c) absorption phenomenon in back-layer and front-layer,(d) half of the size absorbance, (e) step by step design evaluation.

design with the sun-shaped design which helps the structure to capture the radiated incident waves inside the absorber. The proposed structure is also simulated with different scaling in 3D along with the actual scale. The geometrical parameters are scaled down to 50% and scaled up to 200% in all axis's directions. The absorption characteristics are changed as the scale of the structure is altered in the simulation which is depicted in Fig. 2(d). In 50% or half scaling, the structure gives 77.06% absorption with a peak at 390nm. Though the average absorption is not satisfactory with this scaling, the proposed structure can be used as sensors in the visible domain due to its linear decrease in absorption level. In 200% or double scaling, the structure gives 65.06% absorption and the peak absorption occurs at 760nm. So, the set of values of the geometrical parameters in which the proposed structure is designed gives proper absorbance and this set of values must be ensured for practically implementing the proposed unit cell structure for the broad-band absorber.

Fig. 2(e) illustrates the evaluation of the proposed structure design associated with the design steps showed in Fig. 2(a)-2(d) in section 2.2. Each design step produces different absorbance characteristics. The design was modified until the absorbance characteristics are satisfied. In the first step, only with the square-shaped resonator, the average absorption is 91.84% with maximum absorption of 96.02% at 456.70nm. Then, in the second step, in which the circular ring resonator is also introduced, the average absorption becomes 96.16% with maximum absorption of 99.92% at 482.26nm. After that, in the third modification, the average absorption is 95.77% with maximum absorption of 98.79% at 528.05nm. The peak absorption is shifting from left to right for the first three design modifications, respectively. Finally, in the last modification of the suggested design illustrated in Fig. 2(d), the average absorption becomes 96.43% with maximum absorption of 99.99% at the resonant wavelength of 523.22nm. So, it is apparent that the final design possesses the highest average absorption with a near-unity peak which gives a broad-band absorber for the entire visible region, and so, it is the proposed structure for the MMA unit cell.

C. POLARIZATION INDEPENDENCE AND POLARIZATION CONVERSION RATIO (PCR)

All metamaterial absorbers are not used as polarizer converters. To confirm the situation of co and cross-polarization Fig. 3(a) was calculated by (3) and (4). Both X and Y polarized transmission waves get confine in the absorber. It means the transmission coefficients are infinitesimal in magnitude, hence under scrutiny region the waves can't transform.

$$|S(\omega)|^2 = |S_{P,P}(\omega)|^2 + |S_{P,Q}(\omega)|^2 = T^2_{yy} + T^2_{yx} \quad (3)$$

$$|S(\omega)|^2 = |S_{Q,Q}(\omega)|^2 + |S_{Q,P}(\omega)|^2 = T^2_{xx} + T^2_{xy} \quad (4)$$

This article has been accepted for publication in a future issue of this journal, but has not been fully edited. Content may change prior to final publication. Citation information: DOI 10.1109/ACCESS.2021.3111813, IEEE Access

Here, $|S_{P,P}(\omega)|^2 = |S_{Q,Q}(\omega)|^2 = T^2_{yy} = T^2_{xx}$ = X-polarization reflectivity and $|S_{P,Q}(\omega)|2 = |S_{Q,P}(\omega)|^2 = T^2_{yx} = T^2_{xy}$ = Y-polarization reflectivity. PCR is the ratio of X-polarized reflectivity over the total reflectivity. To calculate the PCR (3) and (4) were used. From Fig. 3(b), It can be noticed the PCR vale for transverse electric (PCR_P) and transverse magnetic (PCR_Q) mode are refusable, which completely removes the issue of polarization conversion factors. This is because the T_{xy} is very small in magnitude.

$$PCR_P = T^2_{yx/} (T^2_{yy} + T^2_{yx}) \quad (5)$$

$$PCR_Q = T^2_{xy/} (T^2_{xx} + T^2_{xy}) \quad (6)$$

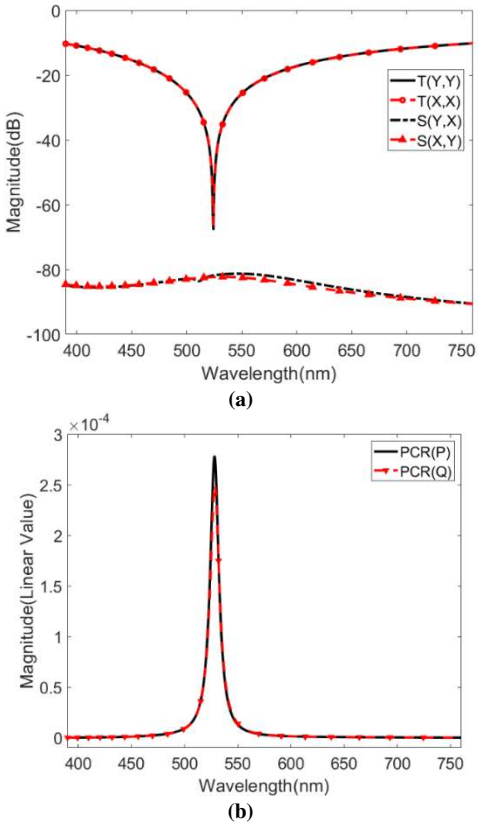

FIGURE 3. (a) Co-polarization and cross-polarization phenomenon, and (b) PCR value of the proposed model in TE and TM mode in PCR (P) and PCR (Q) respectively.

D. NUMERICAL VERIFICATION

To verify the results that are simulated in CST, COMSOL Multiphysics is used with the Finite Element Method (FEM) to give authentication to the simulated results achieved in this research. Numerical verification shows in Fig. 4 that the average absorption holds 96.52% from 390nm to 760nm that goes a little bit high of 0.09% from the simulated one. Maximum absorption is found at 541.1nm having an absorption of 99.36%. It is seen that the absorption peak shift 17.88nm, as well as the absorption, goes down by 0.639%. It seems that the simulated and the verified data give too much similar results and swelling the authentication of the proposed MMA. Thus, it is expected that the proposed MMA also gives desired results in the experimental verification.

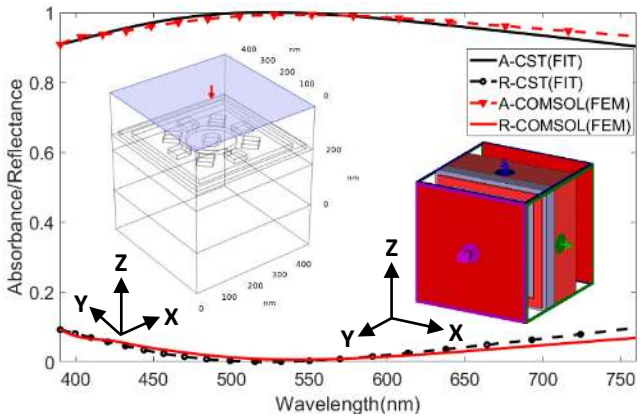

FIGURE 4. Numerical verification with finite element method in COMSOL Multiphysics. Insets: Environment of the proposed model in COMSOL Multiphysics and CST MSW.

E. INCIDENT ANGLE STABILITY AND POLARIZATION INSENSITIVITY

The proposed absorber absorption characteristics were also checked under the consideration of polarization and incident angle of the wave shown in Fig. 5 with the graphical representation of normal and oblique incident angle in Fig. 5(a, b). Polarization is scrutinized with an angle of 0° to 90° in both TE and TM mode. It is shown that from Fig. 5 (c, e) the proposed absorber's absorbance characteristics do not change with the different polarization angle up to 90° and average absorption remains quite similar to the previous one and it can be said that the theoretically developed absorber is independent to polarization i.e. polarization-insensitive. The suggested unit cell consists of a rotationally symmetric fourfold resonator. The polarization insensitivity of the unit cell is due to its vertically and horizontally symmetric features [54]–[56] When it comes to under variation of incident angle absorption characteristics are displayed with a change of 10° incident angle from 0° to 70° in Fig. 5 (d, f) for TE and TM mode. Regarding the variation of the angle of incident average absorption, peak absorption at specific resonance wavelength is given in Table 2 concerning TE and TM mode. Since the absorption is computed using specular reflection, the reflected field intensity reduces by about 10 dB when the receiving incident angle deviates 10 degrees from the normalized direction. The resonator in this work has a circular ring in the middle along with eight slotted sectors around the circular ring that allow for wide-angle insensitivity, and the electric fields are entered on the circular ring's edges and the magnetic fields are large at the slotted sectors as shown in Fig. 8 (a-h) and its parameters have been fine-tuned to have the least degree of angle sensitivity possible [55], [57], [58]. This geometric pattern aids the proposed structure to be wide-angle stable in the visible region.

This article has been accepted for publication in a future issue of this journal, but has not been fully edited. Content may change prior to final publication. Citation information: DOI 10.1109/ACCESS.2021.3111813, IEEE Access

TABLE 2. Average absorption and peak absorption at specific resonance in TE and TM mode under various incident angle

Incident Angle	Average Absorption		Peak Absorption		Resonant Wavelength (nm)	
	TE	TM	TE	TM	TE	TM
0°	96.35%	96.43%	99.999%	99.997%	523.56	528.05
10°	96.59%	96.59%	99.996%	99.996%	520.84	522.88
20°	96.62%	96.61%	99.823%	99.821%	517.14	518.82
30°	96.10%	96.10%	99.346%	99.347%	488.45	490.24
40°	94.55%	94.54%	98.278%	98.279%	473.72	468.73
50°	90.94%	90.93%	95.859%	95.859%	445.77	444.29
60°	83.78%	83.78%	90.834%	90.834%	430.91	426.78
70°	70.28%	70.42%	79.234%	79.246%	427.46	427.46

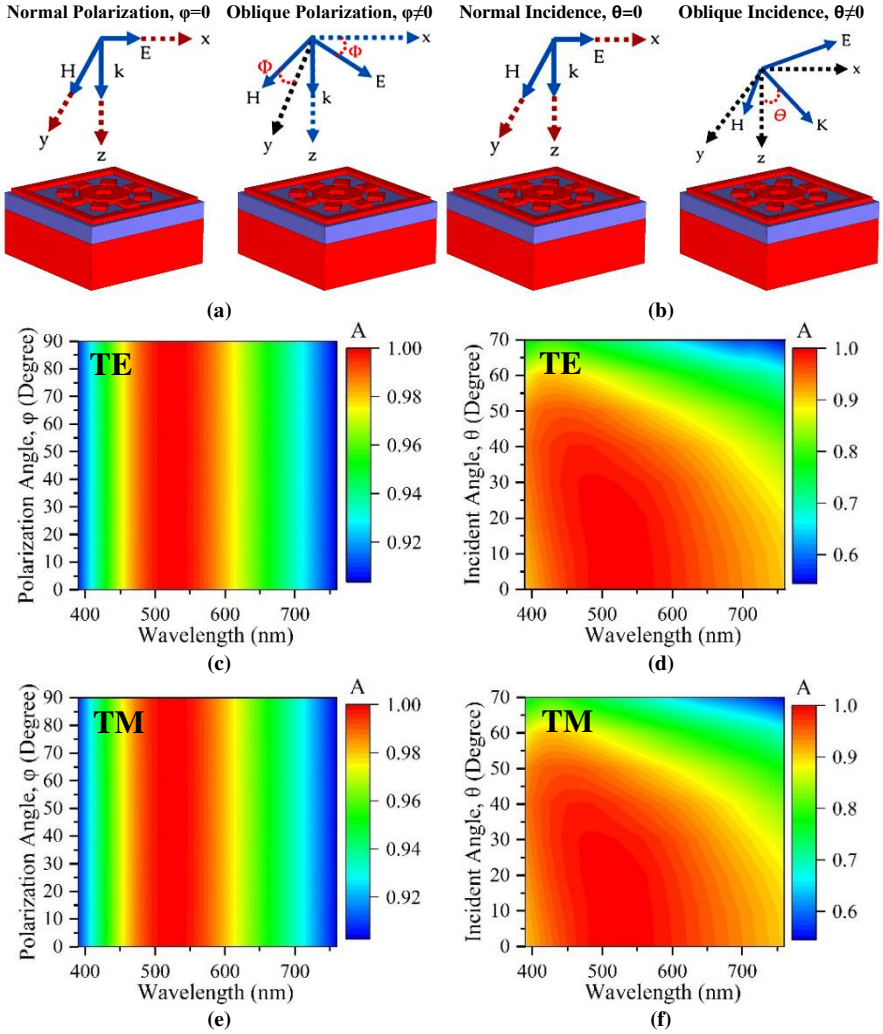

FIGURE 5. Demonstration of (a) normal and oblique polarization angle (b) normal and oblique incident angle (c) polarization angle for TE mode from 0-90°, (d) incident angle for TE mode from 0-70°, (e) polarization angle for TM mode from 0-90°, and (f) incident angle for TM mode from 0-70°.

From table no 02, it can be said that with the change of incident angle from minimum to maximum, absorption decreases, and peak absorption also decreases along with resonance wavelength. Because the higher the incident angle, the longer the path length, and the lower the coupling effect has long been known. This reduced coupling effect decreases the structure's electromagnetic dipolar resonance, resulting in less wave confinement in the dielectric layer [59]. But still, the proposed absorber gives a competitive look with a different incident angle. So, the proposed absorber is a perfect candidate for polarization-insensitive and incident angle stability-based MMA.

This article has been accepted for publication in a future issue of this journal, but has not been fully edited. Content may change prior to final publication. Citation information: DOI 10.1109/ACCESS.2021.3111813, IEEE Access

F. GEOMETRIC PARAMETER SWEEP

In this section, extensive parametric sweep analysis is investigated for different important design parameters. The front layer resonator thickness "tr" is swept for values of 5 to 25nm with an increment of 5nm, and the associated results are illustrated in Fig. 6(a). The average absorptions are found to be varied between 93.2%, and 96.43%. Here, the average absorption is increased as the increase in thickness till 15nm, then again, decreased with the increase of thickness. This is because the resonator thickness affects the impedance matching which is associated with the free space. The better impedance matching is taken place at 15nm thickness at which the structure is designed. At other values, a higher impedance mismatch occurs. Now, the resonance wavelengths for different "tr" values are 444.29nm, 491.44nm, 523.22nm, 557.06nm, and 582.58nm, respectively, with a corresponding absorption peak of 98.51%, 99.83%, 99.99%, 99.75%, and 99.32%, respectively. The resonance wavelength is red-shifted due to the rise of the resonator thickness that is meant to be happened according to the equivalent medium theory [60] as well as model associated with the λ/4 resonance [61]. If the size is come to play with a bigger problem, then the proposed structure can be used with tr=10nm rather than 15nm by reducing resonator size as well as expense, by sacrificing a little average absorption level by 0.27%.

The dielectric spacer thickness "ts" is swept for the values of 45 to 65nm with an increment of 5nm and the corresponding results are illustrated in Fig. 6(b). The average absorptions are varied between 95.58%, and 96.43%, with the increase of "ts" till 55nm, and then the absorption starts to fall. This is because the alteration in the dielectric thickness changes the capacitive and inductive effects between resonator and ground slab. Here, the resonance wavelength is also red-shifted because the dielectric spacer

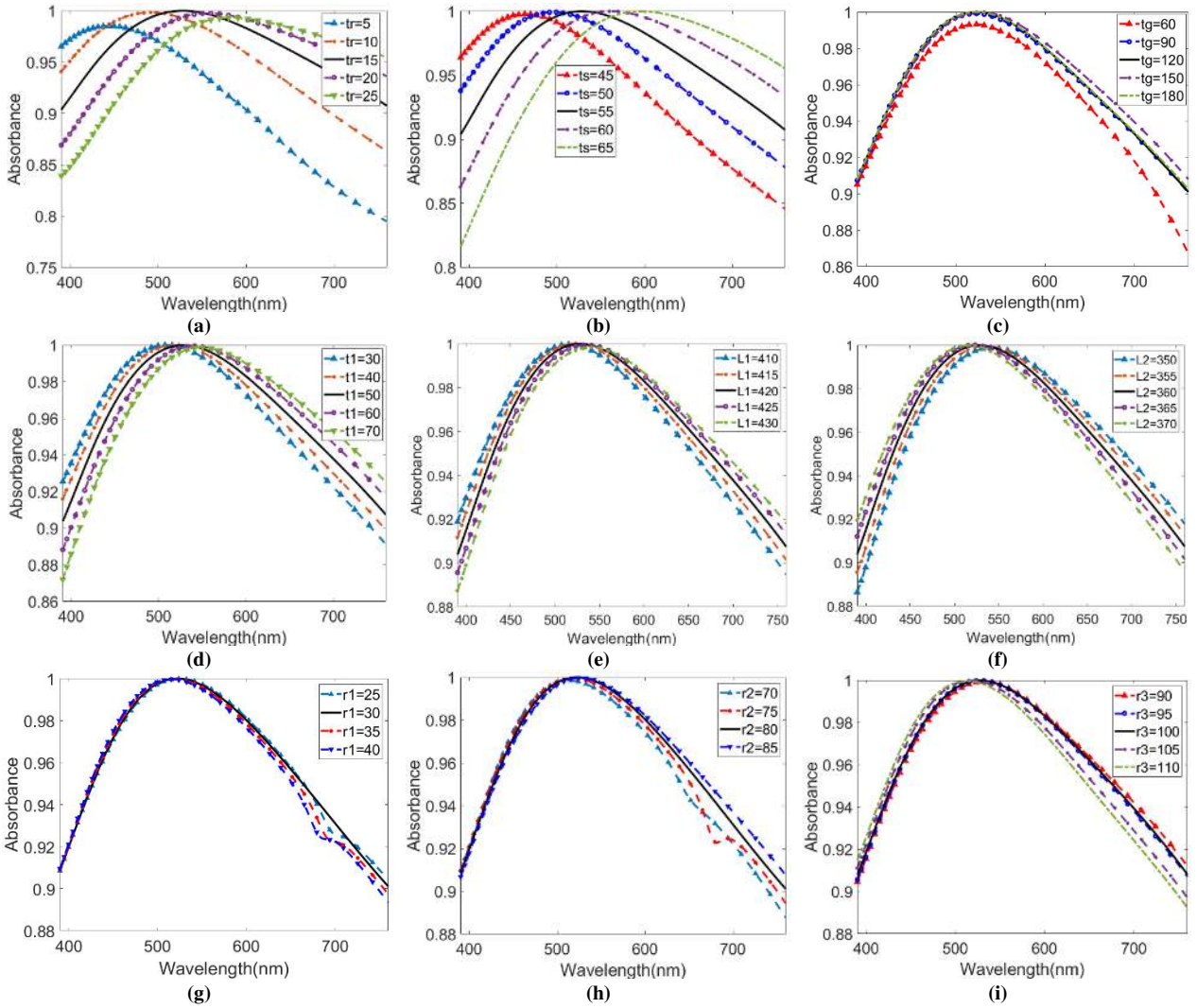

FIGURE 6. Extensive Parametric analysis for parameter (a) thickness of the resonator "tr", (b) thickness of the substrate "ts", (c) thickness of the back-layer "tg", (d) size of the outer shape in resonator "t1", (e) outer length of the square box shape "L1", (f) inner length of the square box shape "L2", (g) outer diameter of the cylinder "r1", (h) inner diameter of the cylinder "r2", and (i) outer radius of the cylindrical cut.

This article has been accepted for publication in a future issue of this journal, but has not been fully edited. Content may change prior to final publication. Citation information: DOI 10.1109/ACCESS.2021.3111813, IEEE Access

thickness affects the ground slab current density and inductance. As the dielectric thickness is increased, the titanium ground slab current density is reduced increased, - the titanium ground slab current density is reduced as well as a decrease in the inductance which results in the red-shifting phenomenon of resonant wavelength [62]. As the average absorptions are very close to each other for ts=50nm and ts=55nm, the proposed structure can be used with 50nm dielectric spacer thickness rather than designed 55nm, by reducing 0.01% average absorption as well as the reduction in dielectric size.

The ground slab thickness "tg" is swept for the values of 60-180nm with a large increment of 30nm which is depicted with absorption characteristics in Fig. 6(c). The average absorptions for this variation are varied between 95.55% and 96.43%. The average absorption is gradually increased with the increase of the tungsten-made ground slab thickness. It is due to the change in blocking of the transmission, and reflect ability with the alteration in the ground layer thickness. As the ground slab is made thicker, the transmission is blocked more efficiently as well as the light is reflected and trapped in the absorber. The resonant wavelength faces a very small red-shift due to the increase of the "tg" values. The absorber can use a thicker tungsten ground slab for broader absorbance but the material cost will increase due to the greater volume of the ground layer.

Fig. 6(d) illustrates the "t1" parameter sweep from 30-70nm with an increment of 10nm. The "t1" parameter is the width of the "sun-ray" shaped resonator parts. The average absorptions are around 96.43% for the first values, and for the last two values, the average absorptions are 96.19%, and 95.85%, respectively. The variation of the average absorption takes place because of the alteration in the capacitance as well as inductance between successive "ray" resonators. There occurs a red-shift in the resonant wavelengths due to the rise in the "t1" values. The proposed design can be used with lower "t1" values as the structure shows broader absorbance.

The effects of change in the side of the outer square "L1" as well as the side of the inner square "L2" are depicted in Fig. 6(e and f), respectively. The "L1" parameter is swept from 410-430nm with an increment of 5nm. The average absorptions are close to 96.43% with slight differences. The resonant wavelengths are red-shifted due to the variation in the impedance matching. The "L2" parameter is swept from 350-370nm with an increment of 5nm, in which the average absorptions are also close to 96.43% with a little difference. Here it is observed that red-shifting occurs in the resonant wavelengths with the increase of "L1". On the other hand, blue-shifting occurs with the increase of the "L2" parameter. It is due to the change in impedance matching properties with the alteration of the square sides. This phenomenon can be utilized in the sensor application for the proposed structure.
The change in the inner radius (R1), outer radius (R2) of the "sun" shaped cylinder, and the "R3" parameter, affects absorption characteristics that are depicted in Fig. 6 (g), Fig. 6(h), and Fig. 6(i), respectively. The "R1" parameter is swept from 20-40nm with an increment of 5nm. The "R2" parameter is swept from 70-90nm with an increment of 5nm. The "R3" parameter is swept from 90-110nm with an increment of 5nm. In all of the cases, the average absorption lies around 96.43%, which is for the actual proposed structure, with a little difference. The resonant wavelength from the "R1" variation faces a little blue-shift phenomenon with the increase in "R1" values, as seen from Fig. 6(g). From the "R2" variation, the resonant wavelength faces a little red-shift phenomenon with the increase in "R2" values, as seen from Fig. (h). For the "R3" alteration, the peak wavelength exhibits a slight blue-shift phenomenon, as seen in Fig. 6 (i). These resonant wavelengths shift of absorber due to parameter change can be utilized in the optical sensor, proximity color detectors, color mapping with the ring radius for artificial intelligent microrobots for biomedical applications, etc.

G. ABSORPTION COMPARISON WITH DIFFERENT METALS AND DIELECTRICS

In this section, different types of absorption phenomena are taken for the proposed design by changing the various dielectric and metal shown in Fig. 7. The resonator and back layer metal (W) were the same in this case of Fig. 7(a). Without SiO_2 (n= 1.5) other four dielectric materials with their corresponding refractive(n) index are GaAs (n= 3.9), Al_3N_4 (n= 2.17), In_2O_3-SnO_2 (n=1.83), and A-Si (n= 4.4) where n is the refractive index. Fig. 7(a) shows that with a change in refractive index the peak absorption also gets changes [63]. In addition, large bandwidth and higher absorption can be obtained with a low refractive index [15]. For the optical region (390nm760nm) light absorption, the selected dielectric material (SiO_2) was so perfect as it has an average absorption of 96.43% with a minimum of 90.2% absorption. Both the GaAs and Amorphous Silicon have a mean absorption of 47.43% and 49.41%, respectively. That's why they can be used for half-power absorption for the mentioned optical region. In_2O_3-SnO_2 can also be used for optical absorption purposes but it will not be as efficient as SiO_2, as it has an average absorption of 88%. AlN can be used as an optical light detector, as it is enhanced linearly for this region.

With the different dielectric sweeps, another attempt was to observe the absorption characteristics with different metal sweeps. We replace the resonator and rear-layer metal with Iron (Fe), Gold (Au), Copper (Cu), Silver (Ag) at the same time. Fig. 7(b) depicts the absorption characteristics with different metals. It is clear that tungsten (W) was the best choice for this design to absorb light as it has a perfect impedance match for this unit cell. Au also shows good absorption from 390nm to 650nm with an average absorption above 93%. Fe, Ag, and Au show multi-band absorption in this case.

This article has been accepted for publication in a future issue of this journal, but has not been fully edited. Content may change prior to final publication. Citation information: DOI 10.1109/ACCESS.2021.3111813, IEEE Access

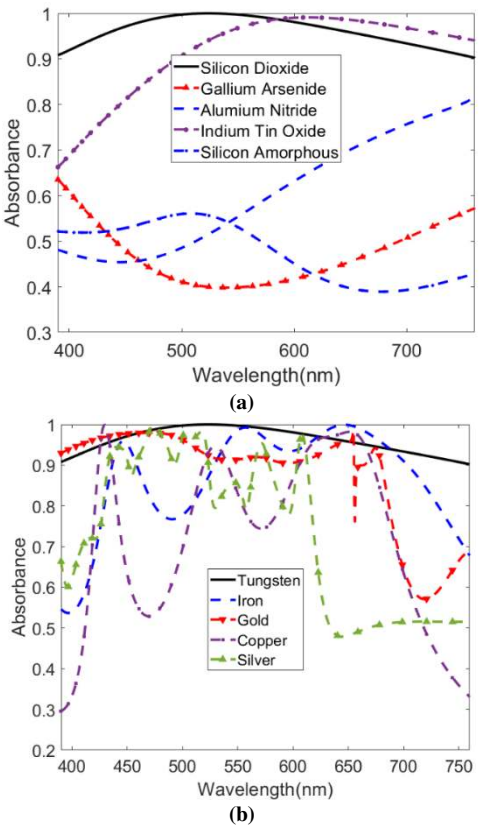

FIGURE 7. Absorption with different (a) dielectric substances, and (b) different metal layers.

H. ELECTRIC AND MAGNETIC FIELD

The analysis of electric field (EF), as well as magnetic field (HF), are shown in Fig. 8, to take care of the physical absorption mechanism with common incidence angle (0°) of EM wave. The EM wave gets condensed and greatly enhanced at some area of the absorber for a given wavelength. The EF and HF are shown here at 523.56nm (A = 99.99%) and 760nm (A = 90.35%) wavelength. For TE and TM polarization, the propagation mode gets altered. The EF and HF for MMA can be described as

$$\mathbf{D}_{avg} = \varepsilon_{eff}\varepsilon_0\mathbf{E}_{avg} \quad (5)$$

$$\mathbf{B}_{avg} = \mu_{eff}\mu_0\mathbf{H}_{avg} \quad (6)$$

Where, D_{avg} = mean electric flux density, ε_{eff} = effective permittivity, ε_0= vacuum permittivity, Eavg = mean EF density, Bavg = Mean magnetic flux-density, μ_{eff} = effective permeability, μ_0 = vacuum permeability, Havg = mean HF density. Integral Maxwell's equation for $\mathbf{D}_{avg}$ and $\mathbf{B}_{avg}$ can stand-with as

$$\int_C \boldsymbol{E}.d\boldsymbol{I} = 0 - \frac{\partial}{\partial t}\iint_S \boldsymbol{B}.d\boldsymbol{S} \quad (7)$$

$$\int_C \boldsymbol{H}.d\boldsymbol{I} = 0 + \frac{\partial}{\partial t}\iint_S \boldsymbol{D}.d\boldsymbol{S} \quad (8)$$

Where, E = EF intensity, D = electric flux density, H = HF density, and B = magnetic flux density. The integral function is computed together with the surface or when the MF shows non-uniform fluctuation rapidly changing after an EM wave

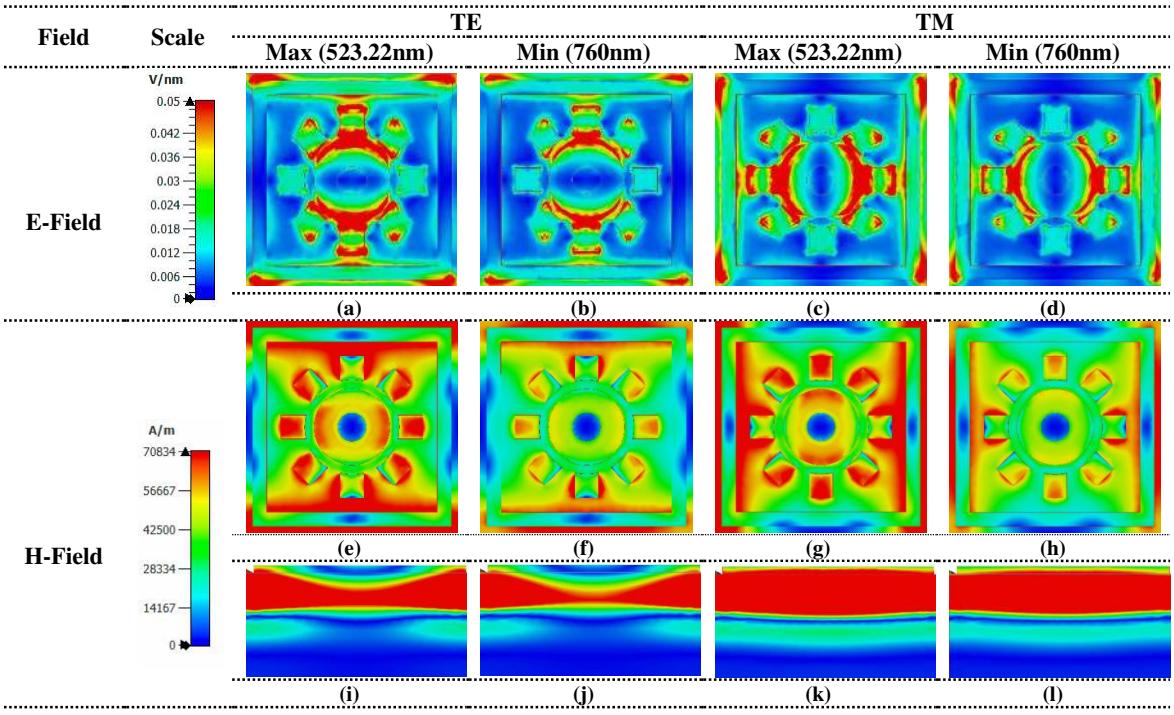

FIGURE 8. Demonstration of maximum point (523.22nm) and minimum point (760nm) (a) - (d) electric field of the proposed model for TE and TM modes with scale bar in V/nm in x-y axis, (e) – (h) magnetic field of the proposed model for TE and TM modes with scale bar in A/m in x-y axis, and (i) – (l) magnetic field in z – y axis with same scale bar in TE and TM modes.

This article has been accepted for publication in a future issue of this journal, but has not been fully edited. Content may change prior to final publication. Citation information: DOI 10.1109/ACCESS.2021.3111813, IEEE Access

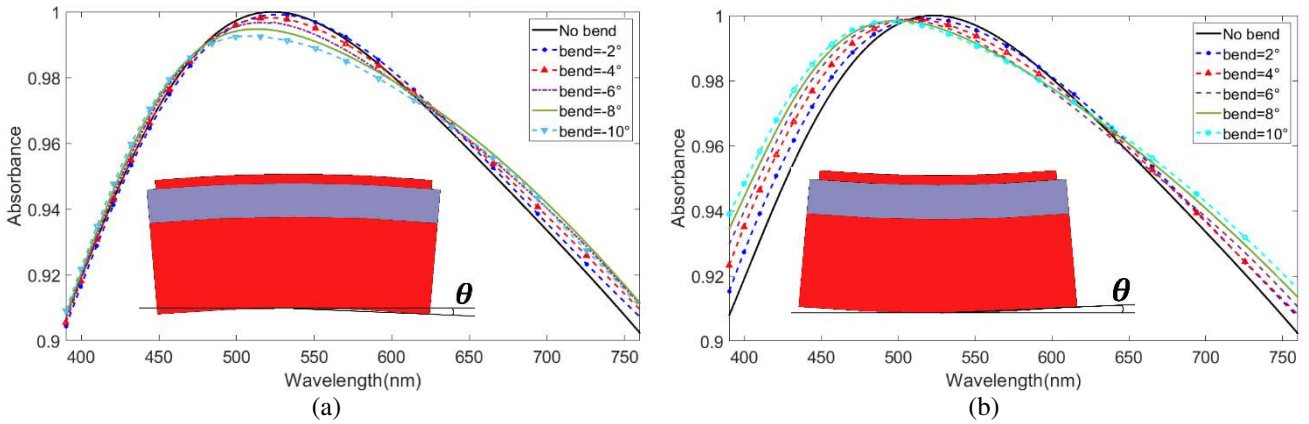

FIGURE 9. Mechanical loading on the proposed unit cell with (a) negative/ convex stress from 0-10º, and (b) positive/concave stress from 0-10º

passes through it. Usually, permittivity reaches unity in a uniform field distribution, however, in this case, H and B are asymmetrical and non - uniform along with the resulting EM wave propagation. The dielectric characteristics (ε, μ) of the nanostructure resonator are determined in this article using the raw method of collecting material parameters from transmission/reflection data [64], [65]. At resonance wavelength, the EF and HF distributions indicate the relevant intense concentrations in certain particular areas of the patch.

Fig. 8(a-d) clearly demonstrates that the EF lies largely between the metal resonator and the dielectric layer interference, especially at the top and lower margins of each resonator slide for transverse electric (TE) polarization as well for Transverse magnetic (TM) the polarization gets altered. This impact increases the surface plasmon which leads the better absorption because these surface plasmons have produced an optimum dipole of resonance for the localized EF [66], [67]. Fig. 8(a,b) shows maximal and minimal EF strength for TE polarization mode, and Fig. 8(c,d) shows maximal and minimal EF strength for TM modes. The intense EF is represented by the redder color. The yellow color denotes moderately dense areas, whereas the blue color denotes less packed areas.

From Fig. 8(e-h), it can be observed that the geometry of the metasurface is accountable for the effect of resonance. There are certain techniques to EM quantities that are suppressed by boundary conditions. The incident wave that penetrates the unit cell gets back-to-back reflection for ground and resonator metal. So, the EM wave is confined at the dielectric spacer mainly [68]. These confined plasmons produce strong HF, hence powerful magnetic dipole can be achieved. EF vectors flow mostly via the dielectric and airspace, creating two current conductor loops that can lead to diamagnetic response and then ignite magnetic polariton's [69], [70]. Fig. 8(e,f) shows the x-y plane HF distributions for lowest and highest absorption for TE mode and Fig. 8(g,h) shows the HF distributions for TM mode. The cross-sectional view of the x-z plane is illustrated in Fig. 8 (i-l). The most intense HF is represented by the redder color. The yellow color and green color denotes areas that are moderately dense, whereas the blue color denotes areas that are less packed. The propagation gets altered with respect to the change of polarization mode.

3.9 MECHANICAL STRESS

Some exterior mechanical effects can arise throughout the course of construction and in the maintenance level of meta-material absorbers [61]. The process entails applying mechanical bending deformations of MMA, accompanied by a numerical modelling analysis of electro-optical features in 390nm to 760nm. The whole structure was bent together from -10º to 10º with a non-uniform mechanical load. The two types of bending, negative bending (Convex bending) and positive bending (Concave bending) [73] absorption analysis for the design showed in Fig. 9. Convex and concave bending are experienced in the unit cell for tensile stress and compression, respectively.

3.9.1 ABSORPTION RESPONSE UNDER CONVEX BENDING

Fig. 9(a) shows the result for convex bending. It can be observed from the illustration, the absorption gets fallen with cumulative convex bending. In addition, the peak absorption shifted from a higher wavelength to a lower wavelength with increasing the bending factor. In terms of convex bending the gap of the resonator gets increased, hence the coupling capacitance gets decreased. So, the resonant frequency (f_R) gets increased. The f_R can be calculated by, $f_R = 1/(2\pi\sqrt{LC})$. Where L is the inductance and C is the capacitance. As the f_R gets increased, so the resonant wavelength gets decreased as $f_R \propto (1/\lambda)$. That's why the peak absorption shifted to the left. Here, for bending angle -10º, -8º, -6º, -4º and -2º the corresponding average absorption are 96.47%, 96.53%, 96.51%, 96.48%, and 96.42% for the mentioned spectrum. Where for no mechanical bending deformation (0º bending) the average absorption was 96.43%. So, the design can be used easily under mechanical deformation, because the average absorption is always above 96.4%.

This article has been accepted for publication in a future issue of this journal, but has not been fully edited. Content may change prior to final publication. Citation information: DOI 10.1109/ACCESS.2021.3111813, IEEE Access

3.9.2 ABSORPTION RESPONSE UNDER CONCAVE BENDING

For concave bending, the average absorptions are more consistent illustrated in Fig. 9(b). Here, concave bending is seen at 2°, 4°, 6°, 8°, and 10°, with average absorption levels of 96.75%, 96.92%, 97.03%, 97.2%, and 97.33%, respectively. Concave bending shifted the peak absorption to the left with increasing the bending effect, similar to the convex bending. Concave bending shows comparatively higher bandwidth absorption than convex bending. This design for the perfect absorption depends on the basis of the nano spilled arm (NSA) physics mechanism. NSA represents the mutual balancing of incoming TEM waves with the split arm of the resonator, as well as the inductance and capacitance of chosen geometry aids in matching with free space impedance.

3.10 COMPARATIVE STUDY OF THE PREVIOUS AND THE PROPOSED DESIGN

A metamaterial absorber with excellent average absorption and wide-angle polarization of incident waves having a compact size is hard to found. Here in Table 3, depending on the absorption band, average absorption, dimension of the unit cell, material choice, and angular stability proposed absorber is compared to other similar visible light absorbers. The proposed broadband absorber with a compact dimension gives an average absorption of 96.43% with a near-unity peak absorption of 99.99% and shows wide-angle polarization insensitivity with the absorption of 70% up to 70°. Thermal stability of the unit cell is the key factor for maintaining the performance of the absorber keeping in mind that Tungsten and Silicon-di-oxide are used as they both have a strong heat absorption capacity. Another key advantage of the proposed absorber is the bending effect and gives up to 10° of bending in the concave or convex direction that makes the difference with other absorbers in a similar context. Perfect absorption -

TABLE 3. Comparative analysis of the proposed unit cell with previous work.

Bandwidth (nm)	Layer	Dimensions (w*l*h) (nm^3)	Materials used	Wide-angle independency up to 70% angularly stable absorption	Absorption level	Average Absorption	Peak absorption	Year & #ref
300	Two	615*615*380	Ni	Yes, $\theta \leq 60°$	Above 85%	92%	99.8%	2018 [74]
340	Three	550*550*165	W, Ni, Rexolite (PS)	Yes, $\theta \leq 45°$	Above 90%	90.98%	99.42%	2018 [75]
459	Three	400*400*245	W, SO_2	Yes, $\theta \leq 60°$	Above 85%	Above 90%	99.9%	2019 [47]
114	Two	400*400*230	Si, Au	Yes, $\theta \leq 60°$	Above 98%	Above 98%	99.9%	2019 [76]
307	Three	500*500*175	Ni, SO_2	Yes, N/A	Above 91%	N/A	99%	2019 [39]
320	Three	1000*1000*225	W, SO_2	Yes, $\theta \leq 60°$	Above 90%	96.7%	99.99%	2020 [15]
350	Three	200*200*135	W, SO_2, PEC	Yes, $\theta \leq 60°$	Above 85%	Above 90%	99%	2020 [58]
219	Three	520*520*180	W, Ni Rexolite (PS)	No	Above 80%	N/A	99.34%	2020 [38]
308	Three	1000*1000*225	W, SO_2	Yes, $\theta \leq 60°$	Above 91.24%	96.77%	99.99%	2020 [59]
210	Three	1000*1000*644	Au, SO_2	Yes, $\theta \leq 80°$	Above 40%	N/A	99.9%	2021 [44]
380	Three	1555*1555*560	A-Si, Ag, ITO	Yes, $\theta \leq 50°$	above 90%	Above 90.1%	99%	2021 [77]
375	Three	1000*1000*165	W, Quartz	Yes, $\theta \leq 45°$	above 66.66%	90%	99.92%	2021 [42]
311	Three	400*400*99	W, SO_2	Yes, $\theta \leq 30°$	Above 85%	92.2%	99%	2021 [45]
370	Three	450*450*220	W, SO_2	Yes, $\theta \leq 70°$	Above 90.2%	96.43%	99.999%	[Proposed]

characteristics, wide-angle polarization insensitivity, material choice, compactness in size, thermal stability, cost-effectiveness makes the absorber unique from the other comparable metamaterial absorber in the optical regime.

IV. CONCLUSION

In short, a three-layer broadband ultrathin, polarization-independent metamaterial absorber having Tungsten (W) based resonator where Silicon-di-oxide (SiO_2) is used as a substrate sandwiched with resonator and bottom plate (W), is designed and described theoretically. The numerical investigation represents that the proposed broadband absorber has an average absorption of 96.43% over 390nm to 770nm with minimum absorption in the investigated range above 90.20% and having near unity peak absorption of 99.999% at 523.22nm. The numerical approach shows that the proposed MMA works in the ultraviolet (UV) region to near-infrared (NIR) region with average absorption above 80%. The numerical study found that Polarization Conversion Ratio (PCR) nearly zero in the desired absorption band thus the proposed absorber shows absorption characteristics independent of the incident wave up to 70° and proposed MMA can minimize the effect of mechanical stress up to 10º insensitivity, thermal stability, it can be an auspicious aspirant for solar energy harvesting, optical sensors, light trapping, and various photonic applications at high temperatures.

AUTHORS CONTRIBUTIONS

Conceptualization, Md Mizan Kabir Shuvo, Sultan Mahmud, and Mohammad T. Islam; Data curation, Md Mizan Kabir Shuvo, Md Imran Hossain, Sydur Rahman, and Sultan Mahmud; Formal analysis, Md Mizan Kabir Shuvo, Sikder Sunbeam Islam, and Sultan Mahmud; Funding acquisition, Mohammad T. Islam; Investigation, Md Imran Hossain, Sultan Mahmud, Sikder Sunbeam Islam, and Mohammad T.

Islam; Methodology, Md Mizan Kabir Shuvo, Sultan Mahmud, and Sikder Sunbeam Islam; Visualization, Md Mizan Kabir Shuvo, Md Imran Hossain, Sikder Sunbeam Islam, and Mohammad T. Islam; Writing – original draft, Md Mizan Kabir Shuvo, Md Imran Hossain, Sydur Rahman, and Sultan Mahmud; Writing – review & editing, Sikder Sunbeam Islam, and Mohammad T. Islam; Software and Resources, Mohammad T. Islam; Supervision, Mohammad T. Islam;

REFERENCES

[1] S. K. V., M. ElKabbash, V. Caligiuri, R. Singh, A. De Luca, and G. Strangi, "Graphene and Topological Insulator-Based Active THz Hyperbolic Metamaterials BT - New Directions in Thin Film Nanophotonics," Singapore: Springer Singapore, 2019, pp. 159–172.

[2] Y.-C. Chang, A. V Kildishev, E. E. Narimanov, and T. B. Norris, "Metasurface perfect absorber based on guided resonance of a photonic hypercrystal," *Phys. Rev. B*, vol. 94, no. 15, p. 155430, Oct. 2016, doi: 10.1103/PhysRevB.94.155430.

[3] V. G. Veselago, "The Electrodynamic of Substances with Simultaneous Negative Values of e and μ," *Sov. Phys. Uspekhi*, vol. 10, no. 4, pp. 509–514, 1968.

[4] J. B. Pendry, "Negative Refraction Makes a Perfect Lens," *Phys. Rev. Lett.*, vol. 85, no. 18, pp. 3966–3969, Oct. 2000, doi: 10.1103/PhysRevLett.85.3966.

[5] B. D. F. Casse, W. T. Lu, Y. J. Huang, E. Gultepe, L. Menon, and S. Sridhar, "Super-resolution imaging using a three-dimensional metamaterials nanolens," *Appl. Phys. Lett.*, vol. 96, no. 2, p. 23114, Jan. 2010, doi: 10.1063/1.3291677.

[6] T. Han, X. Bai, J. T. L. L. Thong, B. Li, and C.-W. W. Qiu, "Full Control and Manipulation of Heat Signatures: Cloaking, Camouflage and Thermal Metamaterials," *Adv. Mater.*, vol. 26, no. 11, pp. 1731–1734, Mar. 2014, doi: https://doi.org/10.1002/adma.201304448.

[7] M. A. Kats and F. Capasso, "Optical absorbers based on strong interference in ultra-thin films (Laser Photonics Rev. 10(5)/2016)," *Laser Photon. Rev.*, vol. 10, no. 5, p. 699, Sep. 2016, doi: https://doi.org/10.1002/lpor.201670055.

[8] K. Du, Q. Li, W. Zhang, Y. Yang, and M. Qiu, "Wavelength and thermal distribution selectable microbolometers based on metamaterial absorbers," *IEEE Photonics J.*, vol. 7, no. 3, 2015, doi: 10.1109/JPHOT.2015.2406763.

[9] X. Chen, Z. Wu, Z. Zhang, and Y. Zou, "Ultra-broadband and wide-angle absorption based on 3D-printed pyramid," *Opt. Laser Technol.*, vol. 124, no. November 2019, p. 105972, 2020, doi: 10.1016/j.optlastec.2019.105972.

[10] M. M. Hasan, M. R. I. Faruque, and M. T. Islam, "Dual band metamaterial antenna for LTE/bluetooth/WiMAX system," *Sci. Rep.*, vol. 8, no. 1, pp. 1–17, 2018, doi: 10.1038/s41598-018-19705-3.

[11] N. Misran, M. T. Islam, M. Y. Ismail, and S. H. Yusop, "Analisis Pencirian Parameter Ketebalan dan Kebertelusan Substrat bagi Elemen Cincin Segiempat Sepusat Bersela Antena Tatasusun Pantulan," *J. Kejuruter.*, vol. 23, no. November, pp. 11–15, 2011.

[12] J. Alam, M. R. I. Faruque, and M. T. Islam, "Labyrinth double split open loop resonator based bandpass filter design for S, C and X-band application," *J. Phys. D. Appl. Phys.*, vol. 51, no. 26, p. 265102, 2018, doi: 10.1088/1361-6463/aac569.

[13] L. Li *et al.*, "Electromagnetic reprogrammable coding-metasurface holograms," *Nat. Commun.*, vol. 8, no. 1, p. 197, 2017, doi: 10.1038/s41467-017-00164-9.

[14] S. Yang, C. Guan, X. Ding, K. Zhang, S. N. Burokur, and Q. Wu, "Fourier convolution operation on metasurface-based hologram in microwave region," *Photonics*, vol. 8, no. 6, 2021, doi: 10.3390/photonics8060174.

[15] S. Mahmud, S. S. Islam, A. F. Almutairi, and M. T. Islam, "A Wide Incident Angle, Ultrathin, Polarization-Insensitive Metamaterial Absorber for Optical Wavelength Applications," *IEEE Access*, vol. 8, no. July, pp. 129525–129541, 2020, doi: 10.1109/ACCESS.2020.3008429.

[16] S. Mahmud *et al.*, "A Multi-Band Near Perfect Polarization and Angular Insensitive Metamaterial Absorber with a Simple Octagonal Resonator for Visible Wavelength," *IEEE Access*, vol. 9, pp. 117746–117760, 2021, doi: 10.1109/access.2021.3106588.

[17] A. Faruk and C. Sabah, "Absorber and sensor applications of complimentary H-shaped fishnet metamaterial for sub-terahertz frequency region," *Optik (Stuttg).*, vol. 177, pp. 64–70, 2019, doi: 10.1016/j.ijleo.2018.09.145.

[18] Y. Ji *et al.*, "High-performance metamaterial sensors based on strong coupling between surface plasmon polaritons and magnetic plasmon resonances," *Results Phys.*, vol. 14, no. May, p. 102397, 2019, doi: 10.1016/j.rinp.2019.102397.

[19] Z. Xiong *et al.*, "Terahertz sensor with resonance enhancement based on square split-ring resonators," *IEEE Access*, pp. 1–1, 2021, doi: 10.1109/access.2021.3073043.

[20] K. Zhang *et al.*, "Polarization-Engineered Noninterleaved Metasurface for Integer and Fractional Orbital Angular Momentum Multiplexing," *Laser Photonics Rev.*, vol. 15, no. 1, pp. 1–10, 2021, doi: 10.1002/lpor.202000351.

[21] Y. Yuan *et al.*, "Independent phase modulation for quadruplex polarization channels enabled by chirality-assisted geometric-phase metasurfaces," *Nat. Commun.*, vol. 11, no. 1, pp. 1–9, 2020, doi: 10.1038/s41467-020-17773-6.

[22] Z. Wang *et al.*, "Dynamic tuning of optical absorbers for accelerated solar-thermal energy storage," *Nat. Commun.*, vol. 8, no. 1, p. 1478, 2017, doi: 10.1038/s41467-017-01618-w.

[23] A. Monti, A. Alù, A. Toscano, and F. Bilotti, "The Design of Optical Circuit-Analog Absorbers through Electrically Small Nanoparticles," *Photonics* , vol. 6, no. 1. 2019, doi: 10.3390/photonics6010026.

[24] Y. C. Song, J. Ding, and C. J. Guo, "A semi-analytical numerical method for fast metamaterial absorber design," *AIP Adv.*, vol. 5, no. 9, 2015, doi: 10.1063/1.4930531.

[25] S. K. Sharma, S. Ghosh, K. V. Srivastava, and A. Shukla, "Ultra-thin dual-band polarization-insensitive conformal metamaterial absorber," *Microw. Opt. Technol. Lett.*, vol. 59, no. 2, pp. 348–353, Feb. 2017, doi: https://doi.org/10.1002/mop.30285.

[26] L. Shi *et al.*, "Ultra-narrow multi-band polarization-insensitive plasmonic perfect absorber for sensing," *Nanotechnology*, vol. 31,

no. 46, p. 465501, 2020, doi: 10.1088/1361-6528/abad60.

[27] J. Li, Y. Yuan, Q. Wu, S. N. Burokur, and K. Zhang, "Dual-band independent phase control based on high efficiency metasurface," *Chinese Opt. Lett.*, vol. 19, p. 100501, Oct. 2021, doi: 10.3788/COL202119.100501.

[28] N. I. Landy, S. Sajuyigbe, J. J. Mock, D. R. Smith, and W. J. Padilla, "Perfect metamaterial absorber," *Phys. Rev. Lett.*, vol. 100, no. 20, pp. 1–4, 2008, doi: 10.1103/PhysRevLett.100.207402.

[29] Q. Feng, M. Pu, C. Hu, and X. Luo, "Engineering the dispersion of metamaterial surface for broadband infrared absorption," *Opt. Lett.*, vol. 37, no. 11, p. 2133, 2012, doi: 10.1364/ol.37.002133.

[30] X. Jiang, T. Wang, Q. Zhong, R. Yan, and X. Huang, "A near-ideal solar selective absorber with strong broadband optical absorption from UV to NIR," *Nanotechnology*, vol. 31, no. 31, p. 315202, 2020, doi: 10.1088/1361-6528/ab88ee.

[31] B. X. Wang, G. Z. Wang, X. Zhai, and L. L. Wang, "Polarization tunable terahertz metamaterial absorber," *IEEE Photonics J.*, vol. 7, no. 4, pp. 1–6, 2015, doi: 10.1109/JPHOT.2015.2448718.

[32] P. Stability, H. Zhai, C. Zhan, Z. Li, C. Liang, and S. Member, "A Triple-Band Ultrathin Metamaterial Absorber With," *IEEE Antennas Wirel. Propag. Lett.*, vol. 14, pp. 241–244, 2015.

[33] G. Liu *et al.*, "Semiconductor meta-surface based perfect light absorber," *Nanotechnology*, vol. 28, no. 16, 2017, doi: 10.1088/1361-6528/aa6613.

[34] H. Song *et al.*, "Near-field coupling and resonant cavity modes in plasmonic nanorod metamaterials," *Nanotechnology*, vol. 27, no. 41, pp. 1–8, 2016, doi: 10.1088/0957-4484/27/41/415708.

[35] Y. Qiu Xu, P. Heng Zhou, H. Bin Zhang, L. Chen, and L. Jiang Deng, "A wide-angle planar metamaterial absorber based on split ring resonator coupling," *J. Appl. Phys.*, vol. 110, no. 4, 2011, doi: 10.1063/1.3622675.

[36] A. Faruk and C. Sabah, "Terahertz metamaterial absorber comprised of H-shaped resonator within split-square ring and its sensory application," *Optik (Stuttg).*, vol. 192, no. March, p. 162976, 2019, doi: 10.1016/j.ijleo.2019.162976.

[37] H. Tong, Y. Xu, Y. Su, and X. Wang, "Theoretical study for fabricating elliptical subwavelength nanohole arrays by higher-order waveguide-mode interference," *Results Phys.*, vol. 14, no. April, p. 102460, 2019, doi: 10.1016/j.rinp.2019.102460.

[38] A. Hoque and M. T. Islam, "Numerical Analysis of Single Negative Broadband Metamaterial Absorber Based on Tri Thin Layer Material in Visible Spectrum for Solar Cell Energy Harvesting," *Plasmonics*, vol. 15, no. 4, pp. 1061–1069, 2020, doi: 10.1007/s11468-020-01132-8.

[39] M. Bagmanci, M. Karaaslan, E. Unal, O. Akgol, M. Baklr, and C. Sabah, "Solar energy harvesting with ultra-broadband metamaterial absorber," *Int. J. Mod. Phys. B*, vol. 33, no. 8, 2019, doi: 10.1142/S0217979219500565.

[40] Y. C. Lai, C. Y. Chen, Y. T. Hung, and C. Y. Chen, "Extending Absorption Edge through the Hybrid Resonator-Based Absorber with Wideband and Near-Perfect Absorption in Visible Region," *Materials (Basel).*, vol. 13, no. 6, 2020, doi: 10.3390/ma13061470.

[41] H. F. Zhang, H. B. Liu, C. X. Hu, and Z. L. Wang, "A Metamaterial Absorber Operating in the Visible Light Band Based on a Cascade Structure," *Plasmonics*, vol. 15, no. 6, pp. 1755–1766, 2020, doi: 10.1007/s11468-020-01190-y.

[42] I. Hossain, M. Samsuzzaman, M. Moniruzzaman, B. B. Bais, M. S. J. Singh, and M. T. Islam, "Polarization-Independent Broadband Optical Regime Metamaterial Absorber for Solar Harvesting: A Numerical Approach," *Chinese J. Phys.*, vol. 71, pp. 699–715, 2021, doi: https://doi.org/10.1016/j.cjph.2021.04.007.

[43] P. Wu, C. Zhang, Y. Tang, B. Liu, and L. Lv, "A perfect absorber based on similar fabry-perot four-band in the visible range," *Nanomaterials*, vol. 10, no. 3, pp. 1–10, 2020, doi: 10.3390/nano10030488.

[44] Y. Zhang *et al.*, "Dual band visible metamaterial absorbers based on four identical ring patches," *Phys. E Low-Dimensional Syst. Nanostructures*, vol. 127, no. November, p. 114526, 2021, doi: 10.1016/j.physe.2020.114526.

[45] S. Charola, S. K. Patel, K. Dalsaniya, R. Jadeja, T. K. Nguyen, and V. Dhasarathan, "Numerical investigation of wideband L-shaped metasurface based solar absorber for visible and ultraviolet region," *Phys. B Condens. Matter*, vol. 601, p. 412503, 2021, doi: 10.1016/j.physb.2020.412503.

[46] Y. Lin *et al.*, "Tungsten based anisotropic metamaterial as an ultra-broadband absorber," *Opt. Mater. Express*, vol. 7, no. 2, p. 606, 2017, doi: 10.1364/ome.7.000606.

[47] C. Cao and Y. Cheng, "A broadband plasmonic light absorber based on a tungsten meander-ring-resonator in visible region," *Appl. Phys. A Mater. Sci. Process.*, vol. 125, no. 1, p. 0, 2019, doi: 10.1007/s00339-018-2310-1.

[48] S. Behera and J. Joseph, "Plasmonic metamaterial based unified broadband absorber/near infrared emitter for thermophotovoltaic system based on hexagonally packed tungsten doughnuts," *J. Appl. Phys.*, vol. 122, no. 19, 2017, doi: 10.1063/1.5003054.

[49] E. G. Gamaly and A. V. Rode, "Transient optical properties of dielectrics and semiconductors excited by an ultrashort laser pulse," *J. Opt. Soc. Am. B*, vol. 31, no. 11, p. C36, 2014, doi: 10.1364/josab.31.000c36.

[50] M. Rauf, A. M. Khan, A. Ansari, M. T. Jilani, and T. Shahzeb, "Skin depth verification of the electromagnetic waves for hydrocarbon detection," *Int. J. Appl. Electromagn. Mech.*, vol. 60, no. 3, pp. 313–326, 2019, doi: 10.3233/JAE-180105.

[51] E. J. Rothwell, J. L. Frasch, S. M. Ellison, P. Chahal, and R. O. Ouedraogo, "Analysis of the Nicolson-Ross-Weir method for characterizing the electromagnetic properties of engineered materials," *Prog. Electromagn. Res.*, vol. 157, no. October, pp. 31–47, 2016, doi: 10.2528/PIER16071706.

[52] M. J. Hossain, M. R. I. Faruque, M. R. Ahmed, M. J. Alam, and M. T. Islam, "Polarization-insensitive infrared-visible perfect metamaterial absorber and permittivity sensor," *Results Phys.*, vol. 14, no. June, p. 102429, 2019, doi: 10.1016/j.rinp.2019.102429.

[53] Z. Li, L. Stan, D. A. Czaplewski, X. Yang, and J. Gao, "Wavelength-selective mid-infrared metamaterial absorbers with multiple tungsten cross resonators," *Opt. Express*, vol. 26, no. 5, p. 5616, 2018, doi: 10.1364/oe.26.005616.

[54] N. T. Trung, D. Lee, H.-K. Sung, and S. Lim, "Angle- and polarization-insensitive metamaterial absorber based on vertical and horizontal symmetric slotted sectors," *Appl. Opt.*, vol. 55, no. 29, p. 8301, 2016, doi: 10.1364/ao.55.008301.

[55] S. Hannan, M. T. Islam, A. F. Almutairi, and M. R. I. Faruque, "Wide Bandwidth Angle- and Polarization-Insensitive Symmetric Metamaterial Absorber for X and Ku Band Applications," *Sci. Rep.*, vol. 10, no. 1, pp. 3–11, 2020, doi: 10.1038/s41598-020-67262-5.

[56] Y. Wang *et al.*, "Triple-band perfect metamaterial absorber with good operating angle polarization tolerance based on split ring arrays," *Results Phys.*, vol. 16, no. November 2019, p. 102951, 2020, doi: 10.1016/j.rinp.2020.102951.

[57] D. Lee, J. G. Hwang, D. Lim, T. Hara, and S. Lim, "Incident Angle- and Polarization-Insensitive Metamaterial Absorber using Circular Sectors," *Sci. Rep.*, vol. 6, pp. 1–8, 2016, doi: 10.1038/srep27155.

[58] R. M. H. Bilal *et al.*, "Elliptical metallic rings-shaped fractal metamaterial absorber in the visible regime," *Sci. Rep.*, vol. 10, no. 1, 2020, doi: 10.1038/s41598-020-71032-8.

[59] S. Mahmud, S. S. Islam, K. Mat, M. E. H. Chowdhury, H. Rmili, and M. T. Islam, "Design and parametric analysis of a wide-angle polarization-insensitive metamaterial absorber with a star shape resonator for optical wavelength applications," *Results Phys.*, vol. 18, no. August, p. 103259, 2020, doi: 10.1016/j.rinp.2020.103259.

[60] D. R. Smith and J. B. Pendry, "Homogenization of metamaterials by field averaging," *J. Opt. Soc. Am. B*, vol. 23, no. 3, p. 391, 2006, doi: 10.1364/josab.23.000391.

[61] X. Chen *et al.*, "An ultra-broadband and lightweight fishnet-like absorber in microwave region," *J. Phys. D. Appl. Phys.*, vol. 51, no. 28, 2018, doi: https://doi.org/10.1088/1361-6463/aac907.

[62] P. Pitchappa, C. P. Ho, P. Kropelnicki, N. Singh, D. L. Kwong, and C. Lee, "Dual band complementary metamaterial absorber in near infrared region," *J. Appl. Phys.*, vol. 115, no. 19, pp. 0–6, 2014, doi: 10.1063/1.4878459.

[63] Z. Yan *et al.*, "Perfect absorption and refractive-index sensing by metasurfaces composed of cross-shaped hole arrays in metal substrate," vol. 11, no. 1, pp. 1–13, 2021, doi: 10.3390/nano11010063.

[64] A. Hoque, M. T. Islam, A. F. Almutairi, T. Alam, M. J. Singh, and N. Amin, "A polarization independent quasi-TEM metamaterial absorber for X and ku band sensing applications," *Sensors (Switzerland)*, vol. 18, no. 12, 2018, doi: 10.3390/s18124209.

[65] D. R. Smith, S. Schultz, P. Markoš, and C. M. Soukoulis, "Determination of effective permittivity and permeability of metamaterials from reflection and transmission coefficients," *Phys. Rev. B - Condens. Matter Mater. Phys.*, vol. 65, no. 19, pp. 1–5, 2002, doi: 10.1103/PhysRevB.65.195104.

[66] H. M. Lee and J. C. Wu, "A wide-angle dual-band infrared perfect absorber based on metaldielectricmetal split square-ring and square array," *J. Phys. D. Appl. Phys.*, vol. 45, no. 20, 2012, doi: 10.1088/0022-3727/45/20/205101.

[67] X. Han, K. He, Z. He, and Z. Zhang, "Tungsten-based highly selective solar absorber using simple nanodisk array," *Opt. Express*, vol. 25, no. 24, p. A1072, 2017, doi: 10.1364/oe.25.0a1072.

[68] H. Cai, Y. Sun, X. Wang, and S. Zhan, "Design of an ultra-broadband near-perfect bilayer grating metamaterial absorber based on genetic algorithm," *Opt. Express*, vol. 28, no. 10, p. 15347, 2020, doi: 10.1364/oe.393423.

[69] Y. M. Qing, H. F. Ma, and T. J. Cui, "Investigation of strong multimode interaction in a graphene-based hybrid coupled plasmonic system," *Carbon N. Y.*, vol. 145, pp. 596–602, 2019, doi: https://doi.org/10.1016/j.carbon.2019.01.058.

[70] Y. M. Qing, H. F. Ma, and T. J. Cui, "Theoretical Analysis of Tunable Multimode Coupling in a Grating-Assisted Double-Layer Graphene Plasmonic System," *ACS Photonics*, vol. 6, no. 11, pp. 2884–2893, Nov. 2019, doi: 10.1021/acsphotonics.9b00956.

[71] C. J. Cleveland and C. Morris, "Section 15 - Photovoltaics," C. J. Cleveland and C. B. T.-H. of E. Morris, Eds. Boston: Elsevier, 2014, pp. 287–302.

[72] A. E. Nikolaenko, N. Papasimakis, A. Chipouline, F. De Angelis, E. Di Fabrizio, and N. I. Zheludev, "THz bandwidth optical switching with carbon nanotube metamaterial," *Opt. Express*, vol. 20, no. 6, pp. 6068–6079, 2012, doi: 10.1364/OE.20.006068.

[73] S. N. Isa *et al.*, "Effects of bending on a flexible metamaterial absorber," *Bull. Electr. Eng. Informatics*, vol. 9, no. 6, pp. 2436–2442, 2020, doi: 10.11591/eei.v9i6.2204.

[74] Y. Zhou, M. Luo, S. Shen, H. Zhang, D. Pu, and L. Chen, "Cost-effective near-perfect absorber at visible frequency based on homogenous meta-surface nickel with two-dimension cylinder array," *Opt. Express*, vol. 26, no. 21, p. 27482, 2018, doi: 10.1364/oe.26.027482.

[75] E. Ünal, M. Bagmancl, M. Karaaslan, O. Akgol, and C. Sabah, "Strong absorption of solar energy by using wide band metamaterial absorber designed with plus-shaped resonators," *Int. J. Mod. Phys. B*, vol. 32, no. 25, pp. 1–13, 2018, doi: 10.1142/S0217979218502752.

[76] Y. Cheng and C. Du, "Broadband plasmonic absorber based on all silicon nanostructure resonators in visible region," *Opt. Mater. (Amst).*, vol. 98, no. September, p. 109441, 2019, doi: 10.1016/j.optmat.2019.109441.

[77] J. Fang and B. Wang, "Optical capture capability enhancement by right-angled triangular visible absorber," *Phys. Lett. A*, vol. 404, p. 127404, 2021, doi: https://doi.org/10.1016/j.physleta.2021.127404.

This article has been accepted for publication in a future issue of this journal, but has not been fully edited. Content may change prior to final publication. Citation information: DOI 10.1109/ACCESS.2021.3111813, IEEE Access

MD MIZAN KABIR SHUVO graduated from the Department of Electrical and Electronic Engineering at Mymensingh Engineering College, University of Dhaka, Bangladesh, with a B. Sc degree in 2021. His undergraduate thesis was on a metamaterial-based broadband absorber for the optical regime, which he completed. His main research interests are metamaterial absorber, MRR, and IoT-based systems.

MD. IMRAN HOSSAIN received his B. Sc degree in Electrical and Electronic Engineering from Mymensingh Engineering College, University of Dhaka, Bangladesh in 2021. His undergraduate thesis, which he accomplished, focused on a metamaterial-based broadband absorber for the optical region. He has been serving as a reviewer for IEEE ACCESS. Metamaterial absorbers, Metamaterial based antennas, Micro ring resonators, microcontroller-based embedded systems, and IoT-based systems are among his key research interests.

SYDUR RAHMAN now pursuing his Master's degree in the Electrical and Electronic department from Bangladesh University of Engineering and Technology (BUET). He received his B. Sc degree from the Department of Electrical and Electronic Engineering, Mymensingh Engineering College, University of Dhaka, Bangladesh, in 2021. His undergraduate thesis was on tuning and optimization of the micro-ring resonator for wavelength selective applications, which he completed. His main research interests are in the micro-ring resonator and metamaterial absorbers for optical applications. He also enjoys developing microcontroller-based embedded systems and IoT-based applications from undergraduate levels.

SULTAN MAHMUD completed his B.Sc. from the Department of Electrical and Electronic Engineering of the International Islamic University Chittagong (IIUC), Bangladesh in 2020. He completed his undergraduate thesis on metamaterial-based absorbers for optical wavelength applications. He is now working on metamaterial absorbers in the optical and microwave ranges with various applications. He has 03 publications with 13 google scholar citations. He has been serving as a reviewer for IEEE ACCESS. His main research interest includes metamaterials, metamaterial absorbers for optical and microwave applications.

SIKDER SUNBEAM ISLAM (Member, IEEE) is currently serving as an Associate Professor & department head in the Department of Electrical and Electronic Engineering in the International Islamic University Chittagong, Bangladesh.

He has completed his Ph.D. in Space Science from the National University of Malaysia, Malaysia in 2017. He received his M.Sc. in Mobile Computing and Communications in 2008 from the University of Greenwich, United Kingdom, and B.Sc. (Electrical and Electronic Engineering) in 2005 from Bangladesh.

He has been serving as a reviewer for several international conferences and journals. He has one published book and many publications in international proceedings and journals. His main research interests include Metamaterial for Communications, Electromagnetic Radiation, and Mobile Computing.

MOHAMMAD TARIQUL ISLAM (Senior Member, IEEE) is currently a Professor with the Department of Electrical, Electronic and Systems Engineering, Universiti Kebangsaan Malaysia (UKM) and a Visiting Professor with the Kyushu Institute of Technology, Japan. He is the author and co-author of about 500 research journal articles, nearly 200 conference articles, and a few book chapters on various topics related to antennas, metamaterials, and microwave imaging with 22 inventory patents filed. Thus far, his publications have been cited 7300 times and his H-index is 41 (Source: Scopus). His Google scholar citation is 11,000 and his H-index is 48. He was a recipient of more than 40 research grants from the Malaysian Ministry of Science, Technology and Innovation, Ministry of Education, UKM research grant, international research grants from Japan, Saudi Arabia, and Kuwait. His research interests include communication antenna design, metamaterial, satellite antennas, and microwave imaging. Dr. Islam has been serving as an Executive Committee member for IEEE AP/MTT/EMC Malaysia Chapter, since 2019-2020, the Chartered Professional Engineer (CEng), a fellow of IET, U.K., and a Senior Member of IEICE, Japan. He received several International Gold Medal awards, the Best Invention in Telecommunication Award for his research and innovation, and the best researcher awards at UKM. He was a recipient of 2018, 2019, and 2020 IEEE AP/MTT/EMC Malaysia Chapter, Excellent Award. He also won the best innovation award and the Best Research Group in ICT niche by UKM, in different years. He was a recipient of the Publication Award from the Malaysian Space Agency, in several years. He has supervised about 30 Ph.D. theses, 20 M.Sc. theses, and has mentored more than 10 postdocs and Visiting scholars. He has developed the Antenna Measurement Laboratory which includes antenna design and measurement facility till 40 GHz. He was an Associate Editor of IET Electronics Letter. He also serves as the Guest Editor for, SENSORS journal, and an Associate Editor for IEEE ACCESS.